Journal of JSEM, Vol.10, Special Issue (2010) 261-266

Three-dimensional *In Vivo* Contact Analysis of the Wrist Joint during Wrist Motion

Keisuke SASAGAWA[1], Makoto SAKAMOTO[2], Hidenori YOSHIDA[2], Koichi KOBAYASHI[2] and Yuji TANABE[1]

[1] Department of Mechanical and Production Engineering, Niigata University, Niigata 950-2181, Japan
[2]Department of Health Sciences, Niigata University School of Medicine, Niigata, Japan

(*Received 16 February 2010; received in revised form 24 May 2010; accepted 12 June 2010*)

Abstract
The wrist joint is condyloid and capable of movement through two axes: palmar/dorsal flexion and radial/ulnar deviation. Knowledge of *in vivo* joint mechanics is important for understanding pathological mechanisms and the treatment of various joint problems. The purpose of this study was to investigate the *in vivo* wrist joint mechanism during wrist motion. *In vivo* wrist joint contact and the kinematics of the scaphoid and lunate during palmar/dorsal flexion and radial/ulnar deviation were examined using magnetic resonance imaging (MRI). The wrist joints of 15 healthy young volunteers were scanned at 8 positions (–30 deg of palmar flexion; neutral; 30, 60, and 90 deg of dorsal flexion; –20 deg of radial deviation; neutral; and 20 deg of ulnar deviation). Contact of the wrist joint was estimated quantitatively from the derived MR images. Using three-dimensional surface models of the carpal bones, the kinematics of the scaphoid and lunate were analyzed three-dimensionally.

Key words
Wrist Joint, Contact Analysis, Kinematics, Palmar/Dorsal Flexion, Radial/Ulnar Deviation, MRI

1. Introduction

The wrist is a complex joint, consisting of the eight small carpal bones that articulate with each other, the metacarpals distally, and the radius, ulna, and triangular fibrocartilage complex proximally. The eight bones of the wrist represent a highly complex mechanical structure. Each carpal bone moves within 6 deg of freedom for any given wrist motion. Thus, analyzing carpal movement is difficult because of the anatomic and functional characteristics of the wrist.

In vivo biomechanical analysis of the wrist joint is of scientific and clinical relevance because a multitude of clinical problems are related to alterations in normal kinematic behavior. Knirk et al. [1] reported the frequency of post-traumatic arthritis of the wrist after intra-articular fractures of the distal radius as 40–65%. The development of arthritis following displaced intra-articular fractures is attributed to a variety of factors, including initial trauma to the cartilage and elevated contact stresses [2]. Knowledge of *in vivo* joint mechanics is important for understanding pathological mechanisms and the treatment of various joint problems.

To examine the biomechanical properties of the wrist joint, *in vitro* cadaveric studies have been performed using various techniques [3–15]. Pressure-sensitive film and thin-film electronic pressure sensors enable the measurement of pressure distribution, contact area, and contact force [3–7]. Techniques such as bipolar radiography [8–10], electromagnetic sensors [11], and the acquisition of high-speed video data [12,13] have been employed to obtain the kinematic parameters of the carpal bones. These techniques are applicable for cadaveric studies only. *In vivo* studies that seek to investigate kinematic data are performed mainly by computed tomography (CT). CT scanning is an excellent technique for describing bone structure and geometry non-invasively. Three-dimensional (3-D) surface models of bones can be reconstructed from the derived CT image set (CT model) and have been used to analyze 3-D kinematics of the carpal bone [14–19]. Because a CT model is a bone surface model, it cannot examine *in vivo* contact between the cartilages. Joint contact has been analyzed theoretically [20,21].

Magnetic resonance imaging (MRI) has attracted attention for the *in vivo* study of human joint mechanisms. MRI can visualize soft tissue such as cartilage and muscle, as well as contact between the cartilages within the wrist joint. In vivo contact analysis has focused for the weight-bearing joint such as patellofemoral joint [22], knee joint [23] and ankle joint [24]. Pillai et al. [25] estimated *in vivo* joint contact of the wrist and kinematics of the carpal bones during light grasping, but provided no information regarding *in vivo* contact of the wrist joint during wrist motion. The in vivo joint contact distribution during wrist motion is still unknown. The purpose of this study was to investigate the *in vivo* wrist joint mechanism during wrist motion using MRI. We focused on the radioscaphoid and radiolunate joints. *In vivo* wrist joint contact and the kinematics of the scaphoid and lunate during palmar/dorsal flexion (flexion/extension) and radial/ulnar deviation were examined.

2. Materials and Methods

2.1 Image acquisition

Fifteen human participants (mean age, 23.6 ± 2.3 years; 12 males, 3 females) with no previous history of bone or joint disease were enrolled in this study. Informed consent to participate was obtained from all subjects prior to enrollment. Their left wrists were scanned using a 1.5 T MRI system (Achieva, Philips Medical Systems, The Netherlands) and a surface coil. A sequence utilizing the principle of selective excitation was used for clear visualization of cartilage (TR = 20 msec, TE = 8.2 msec, flip angle = 25 deg). The wrist joint was scanned at five positions during palmar/dorsal flexion (–30 deg of palmar flexion, neutral, and 30, 60, and 90 deg of dorsal flexion) and three positions during radial/ulnar deviation (–20 deg of radial deviation, neutral, and 20 deg of ulnar deviation) (Fig. 1). Custom-made devices that did not affect MR scanning were used to reduce motion artifact during image acquisition. Wrist images were acquired in the coronal plane. The field

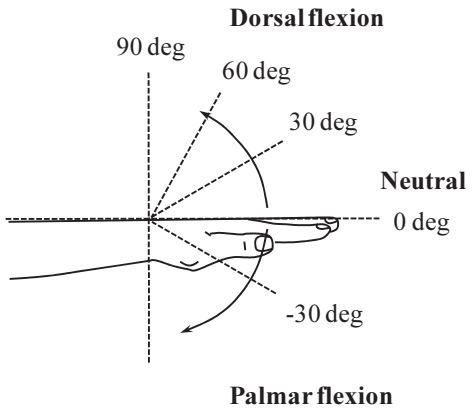

(a) Palmar/dorsal flexion

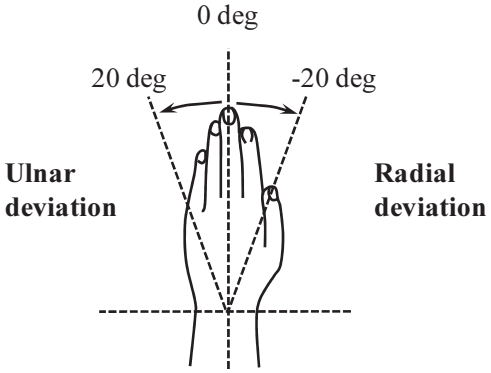

(b) Radial/ulnar deviation

Fig. 1 Scanning position of the wrist joint. A neutral position of the wrist is defined as zero

of view (FOV) was 100 mm with a matrix of 512 × 512, slice thickness of 0.5 mm, and scan time of ~6 minutes.

2.2 Joint contact analysis

Joint contact area was determined by measuring the length of visible contact between the radius and scaphoid, and the radius and lunate in each slice (Fig. 2), multiplying this length by the slice thickness (0.5 mm), and then summing these values to obtain the total contact area (mm^2) [26]. This method is highly reproducible and comparable to established pressure-sensitive film techniques [27]. A single examiner performed all contact area measurements, repeating each measurement four times per scan, to obtain an average contact area for each wrist position and condition.

2.3 Reconstruction of three-dimensional surface models

Three-dimensional surface models of the scaphoid, lunate, and radius, including cartilage surface data, were reconstructed from the MR image sets using a commercial software package (ZedView DB 5.5, Lexi, Japan). Segmentation of bone and cartilage regions was performed manually. Three-dimensional surface models of bone with cartilage were used in the creation of joint-contact distribution maps and in motion analysis of the scaphoid and lunate.

Fig. 2 Typical coronal MR image used for calculating contact area. R: radius, S: scaphoid, L: lunate

2.4 Motion analysis

The kinematics of the scaphoid and lunate were evaluated using registration techniques. Registration was performed under the assumption that each bone moved independently as a 3-D rigid body. The kinematic parameters were calculated by registering 3-D bone models. We used the iterative closest point (ICP) algorithm [28], which is one of the most well-developed methods for surface-based registration. In this method, a 3-D surface model and a set of 3-D points are registered, starting from the initial transformation parameters, to find the best parameters while minimizing the sum of the distance from each 3D point to the surface. The radius was registered with the scaphoid and lunate. Relative motion between the radius and scaphoid and between the radius and lunate were determined by this technique.

To enable quantitative comparison of different wrist postures, we used an anatomic reference coordinate system derived from the distal radius in the neutral position, based on the principal axes of the radius [17]. Using this system, X was the palmar/dorsal flexion axis with positive dorsal flexion, Y was radial/ulnar deviation with positive ulnar deviation, and Z was the pronation/supination axis with positive supination. Helical axis motion and Euler angles were calculated from the neutral position to various wrist positions for the scaphoid and lunate relative to the radius. Euler angles were calculated relative to the anatomic reference coordinate system. Helical axis motion is a method of describing positional change broken down into a rotation about and a translation along an instantaneous axis of rotation [29].

We performed preliminary tests to determine the accuracy of the proposed *in vivo* methodology, using three spherical markers with known relative positions. A 3-D surface model of the markers was reconstructed from the MR images, and the relative positions between the actual markers and the 3-D marker models were compared. The relative position of the 3-D marker models was obtained by registration of each sphere. The distance between two markers and the angle formed by three markers were defined as error of translation and error of rotation,

respectively. The mean errors of translation and rotation for this method were 0.4 mm and 0.3 deg, respectively.

3. Results

Typical joint-contact distribution maps for the articular surface of the radius during wrist motion are shown in Fig. 3. The scaphoid fossa and lunate fossa are located on the articular surface of the radius. In most wrist postures, the scaphoid fossa had larger contact area than did the lunate fossa. During palmar/dorsal flexion, the contact area on the palmar side of the scaphoid fossa moved dorsally. During radial/ulnar deviation, there was no movement of the contact area on the scaphoid fossa. There was a wide distribution of contact areas of the scaphoid fossa from the palmar to the dorsal side, whereas contact area during palmar/dorsal flexion was found on the palmar side or the dorsal side. In participant #2, there was little contact of the lunate fossa during palmar/dorsal flexion. It was noted that joint contacts were dependent on individual anatomy. We calculated the average contact areas during palmar/dorsal flexion and radial/ulnar deviation (Fig. 4). At neutral palmar/dorsal flexion, the mean contact areas of the radioscaphoid and radiolunate joints were 43.6 ± 13.6 and 14.3 ± 16.5 mm^2, respectively. The radioscaphoid contact area was much greater than the radiolunate contact area. The contact areas at radial and ulnar deviation were greater than those at palmar and dorsal flexion. The joint contact area increased with increasing wrist angle during wrist motion.

Sagittal views of the radioscaphoid and the radiolunate joint during palmar/dorsal flexion and radial/ulnar deviation are shown in Fig. 5. The scaphoid and lunate were extended during movement from palmar flexion to dorsal flexion. During ulnar deviation, the scaphoid and lunate were extended. There was greater rotation of these bones at ulnar deviation than at radial deviation. Mean wrist flexions for the scaphoid and lunate at –30 deg of palmar flexion relative to neutral position were –20.2 ± 8.7 deg and –11.2 ± 7.5 deg, respectively (Table 1). Mean wrist extensions for the scaphoid and lunate at 90 deg of dorsal flexion relative to neutral position were 62.9 ± 12.7 deg and 42.0 ± 6.3 deg, respectively. Although the motions of those bones at 30 and 60 deg of dorsal flexion were mainly in-plane motion, their motions at palmar flexion and 90 deg of dorsal flexion were a combination of in-plane and out-of-plane motion. The in-plane motions in radial/ulnar deviation were small, but rotation around the palmar/dorsal flexion axis (out-of-plane motion) was large. For the scaphoid, rotation around the palmar/dorsal flexion axis at radial and ulnar deviations was –1.9 ± 5.2 deg and 19.2 ± 11.5 deg, respectively. Palmar/dorsal flexion axis rotation for the lunate was –1.6 ± 4.2 deg at radial deviation and 18.9 ± 9.4 deg at ulnar deviation. The helical axis parameters during wrist motion (see Table 2) indicate that rotation around the helical axis was similar to that around the palmar/dorsal flexion axis.

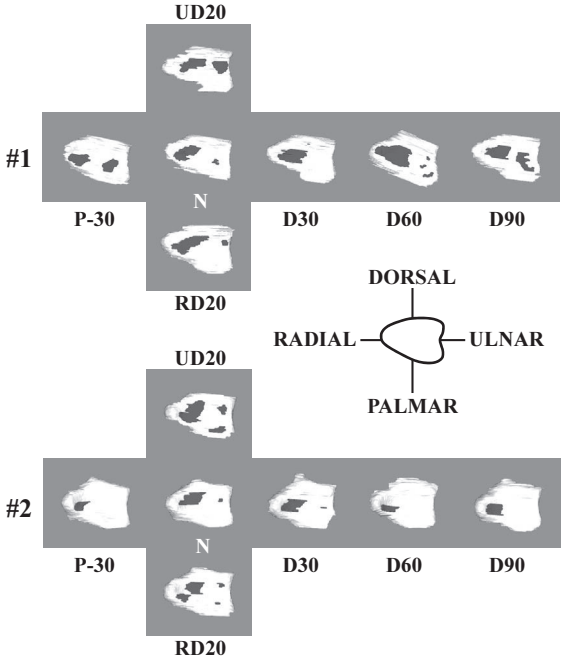

Fig. 3 Typical joint-contact distribution maps of the radius during wrist motion. The scaphoid fossa (left) and lunate fossa (right) are located on the articular surface of the radius. N, neutral; P, palmar flexion; D, dorsal flexion; RD, radial deviation; UD, ulnar deviation

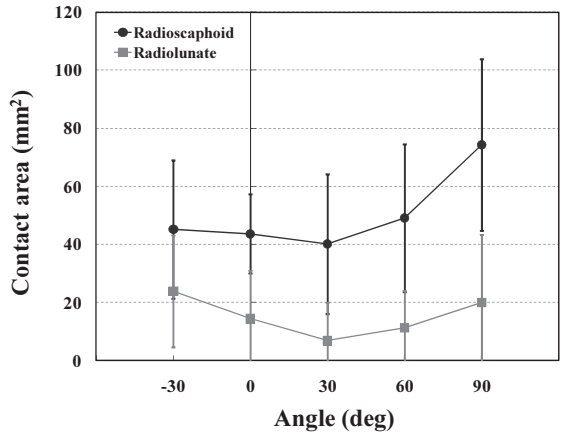

(a) Palmar/dorsal flexion (n = 15)

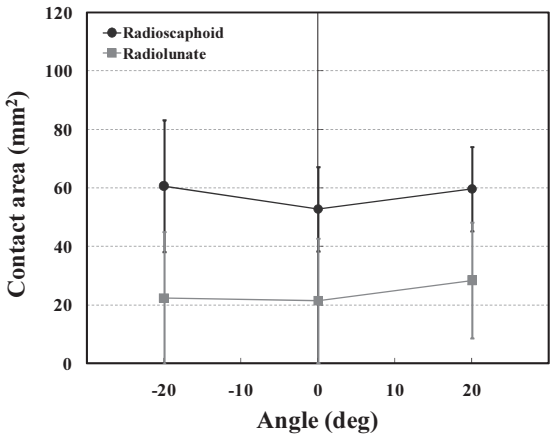

(b) Radial/ulnar deviation (n = 8)

Fig. 4 Changes in radioscaphoid and radiolunate contact areas during wrist motion

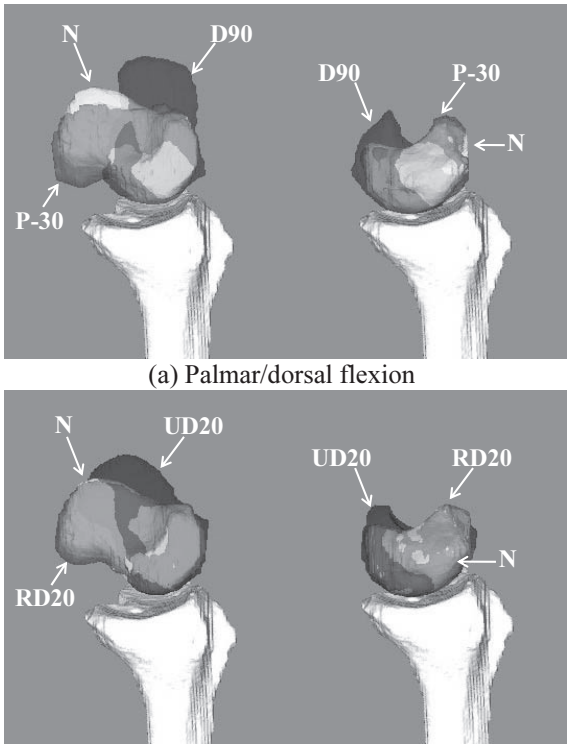

(a) Palmar/dorsal flexion

(b) Radial/ulnar deviation

Fig. 5 Sagittal view of the radioscaphoid (left) and radiolunate joint (right) during wrist motion. N, neutral; P, palmar flexion; D, dorsal flexion; RD, radial deviation; UD, ulnar deviation

4. Discussion

This study represents an attempt to analyze the biomechanical properties of the wrist *in vivo* and non-invasively. MR scanning is a powerful method for imaging soft tissues without radiation; however, it is difficult to depict bone structure using MRI. Sasagawa et al. [30] investigated the accuracy of 3-D MRI-based bone surface models in comparison with an actual bone. They reported that the surface error in the 3-D MRI-based bone model was 1.1 mm. This indicates the potential of 3-D MRI-based bone models for the *in vivo* investigation of joint mechanisms.

To investigate the mechanism of wrist joint contact, Tencer et al. [4] performed cadaveric studies of palmar/dorsal flexion and radial/ulnar deviation, reporting that the ratio of the radioscaphoid contact area to that of the radiolunate was 0.49 in 20 deg of radial deviation, 0.27 in the neutral position, and 1.49 in 10 deg of ulnar deviation. In the present study, the radiolunate–radioscaphoid contact area ratio was 0.44 in radial deviation, 0.41 in the neutral position, and 0.50 in ulnar deviation. The present result for ulnar deviation was less than that reported by Tencer et al. [4]. Investigation into

Table 2 Helical axis-of-motion results. R, rotation about an instantaneous axis; T, translation along an instantaneous axis of rotation; P, palmar flexion; D, dorsal flexion; RD, radial deviation; UD, ulnar deviation

Wrist posture	Scaphoid		Lunate	
	R (deg)	T (mm)	R (deg)	T (mm)
P-30	-21.8 (9.3)	0.9 (2.1)	-13.0 (7.4)	-0.6 (0.9)
D30	23.3 (9.2)	0.4 (0.8)	15.7 (9.1)	-0.1 (0.6)
D60	44.4 (7.8)	1.3 (0.7)	32.1 (6.1)	0.6 (0.9)
D90	65.2 (13.8)	2.4 (0.7)	43.9 (6.2)	1.6 (0.9)
RD20	6.9 (2.7)	2.6 (4.4)	4.9 (3.2)	-0.1 (2.1)
UD20	20.3 (12.1)	1.1 (0.9)	19.8 (9.7)	0.4 (0.7)

The values in parenthesis indicate the standard deviation

Table 1 Scaphoid and lunate motion relative to radius. P, palmar flexion; D, dorsal flexion; RD, radial deviation; UD, ulnar deviation

Wrist posture	Scaphoid relative to radius						Lunate relative to radius					
	Rotation (deg)			Translation (mm)			Rotation (deg)			Translation (mm)		
	θX	θY	θZ	tX	tY	tZ	θX	θY	θZ	tX	tY	tZ
P-30	-20.2 (8.7)	5.8 (3.8)	-0.7 (3.5)	1.3 (0.8)	-3.4 (1.6)	-1.4 (1.0)	-11.2 (7.5)	5.8 (2.9)	0.3 (2.8)	1.3 (0.8)	-1.5 (1.4)	-2.1 (0.9)
D30	20.8 (9.2)	-1.6 (4.5)	0.4 (2.0)	-0.1 (0.8)	2.5 (1.0)	2.4 (1.3)	13.4 (8.7)	-0.7 (3.8)	0.3 (1.5)	-0.3 (0.5)	1.5 (1.0)	2.0 (1.1)
D60	40.8 (9.1)	0.6 (7.5)	-0.9 (4.5)	1.1 (1.7)	4.4 (1.3)	5.1 (1.3)	29.6 (6.7)	1.1 (6.4)	-0.7 (2.6)	0.6 (1.3)	3.0 (0.7)	3.7 (1.0)
D90	62.9 (12.7)	2.6 (9.0)	0.4 (6.7)	2.0 (2.1)	5.1 (1.5)	8.4 (2.5)	42.0 (6.3)	1.5 (7.0)	-1.2 (4.1)	1.7 (1.5)	3.5 (1.0)	5.6 (1.5)
RD-20	-1.9 (5.2)	-1.3 (3.0)	-2.4 (2.8)	0.1 (0.5)	-0.2 (1.0)	-0.2 (0.6)	-1.6 (4.2)	-1.1 (2.4)	-0.3 (2.4)	-0.3 (0.6)	-0.4 (0.5)	-0.1 (0.7)
UD20	19.2 (11.5)	4.9 (3.9)	-2.5 (2.5)	1.7 (1.0)	2.7 (1.4)	1.8 (1.5)	18.9 (9.4)	6.0 (3.6)	-2.5 (2.2)	1.2 (0.8)	2.7 (1.0)	1.5 (1.1)

All values are relative to the neutral position. The values in parenthesis indicate the standard deviation
Rotation: θX, palmar (–) and dorsal (+) flexion; θY, radial (–) and ulnar (+) deviation; θZ, pronation (–) and supination (+)

the mechanism of joint contact is influenced by soft tissue constraints such as muscles, ligaments, and tendons; thus, to understand the mechanism in detail during wrist motion, an *in vivo* study is necessary. A number of theoretical studies have evaluated joint contact of the wrist using CT: the *in vivo* study of Pillai et al. [25] estimated *in vivo* joint contact of the wrist and kinematics of the carpal bones during light grasping, but provided no information regarding *in vivo* contact of the wrist joint during wrist motion, such as palmar/dorsal flexion and radial/ulnar deviation. *In vivo* joint contact can be directly observed on MR images. We believe that estimation of joint contact from MR images includes the influence of soft tissue constraints.

Kaufmann et al. [14,15] examined the helical axis motion parameters for the scaphoid and lunate at flexion/extension and radial/ulnar deviation. At flexion and extension, the rotation angles for the scaphoid relative to the radius were 53 deg and 46 deg, respectively. For the lunate, the rotation angles were 36 deg and 26 deg, respectively. At radial and ulnar deviation, the rotation angles for the scaphoid relative to the radius were 12 deg and 24 deg, respectively. For the lunate, the rotation angles were 10 deg and 29 deg, respectively. Moojen et al. reported movement of the scaphoid and lunate during flexion/extension and radial/ulnar deviation [17,19]. The present results showed a similar tendency to those reported by Kaufmann et al. [14,15] and Moojen et al. [17,19].

In the present study, we observed the movement of contact distribution on the radial articular surface during wrist motion. Joint contact is closely related to the relative position between bones that constitute a joint. Movement of the contact distribution of the wrist joint occurred during motion of the scaphoid and lunate. Joint contact distribution was altered during palmar/dorsal flexion because of the large amount of motion of the scaphoid and lunate; given the reduced rotation during radial/ulnar deviation, there was little change in joint contact distribution during this movement. We found that the contact areas on the lunate fossa were smaller than those on the scaphoid fossa. These differences in contact area express differences in force transmission, and may indicate that force applied to the wrist is transmitted through the scaphoid to a greater degree than through the lunate. The present study demonstrates that our methodology provides useful information regarding joint contact of the wrist.

A limitation of our study is that the contact area of the wrist joint is underestimated. Because of the partial volume effect of MRI, it is difficult to precisely determine the contour of the cartilage. An *in vitro* study is necessary to validate estimates of joint contact. Another limitation is that segmentation of bone and cartilage, and reconstruction of the 3-D MRI-based model is enormously time-consuming. The motion of the carpal bones during wrist motion is influenced by ligaments and tendons; therefore, additional research that takes the soft tissues into account is necessary to understand the mechanism of joint contact.

5. Conclusion

We investigated the joint mechanism of the human wrist *in vivo* using MRI, and performed quantitative analysis of the contact areas on the radial articular surface and the kinematics of the scaphoid and lunate during palmar/dorsal flexion and radial/ulnar deviation. In most wrist postures, the contact areas on the scaphoid fossa were greater than those on the lunate fossa. The joint contact area increased with increasing wrist angle during wrist motion. When rotation of the scaphoid and lunate was greater, as during palmar/dorsal flexion, movement of the contact area was observed.

References

[1] Knirk, J.L. and Jupiter, J.B.: Intra-articular fractures of the distal end of the radius in young adults, *Journal of Bone and Joint Surgery* **68A** (1986), 647-659.

[2] Radin, E.L., Martin, R.B., Burr, D.B., Caterson, B., Boyd, R.D. and Goodwin, C.: Mechanical factors influencing cartilage damage, Osteoarthritis, Current Clinical and Fundamental Problems. Peyron, J.G. (ed.), CIBA-Geigy, France (1985), 90-99.

[3] Viegas, S.F., Tencer, A.F., Cantrell, J., Chang, M., Clegg, P., Hicks, C., O'Meara, C. and Williamson, J.B.: Load Transfer Characteristics of the Wrist. I: The Normal Joint, *Journal of Hand Surgery*, **12A** (1987), 971-978.

[4] Tencer, A.F., Viegas, S.F., Cantrell, J., Chang, M., Clegg, P., Hicks, C., O'Meara, C. and Williamson, J.B.: Pressure Distribution in the Wrist Joint, *Journal of Orthopedic Research*, **6** (1988), 509-517.

[5] Kazuki, K., Kusunoki, M. and Shimazu, A.: Pressure Distribution in the Radiocarpal Joint Measured with A Densitometer Designed for Pressure-Sensitive Film, *Journal of Hand Surgery*, **16A** (1991), 401-408.

[6] Wagner, W.F., Tencer, A.F., Kiser, P. and Trumble, T.E.: Effects of Intra-Articular Distal Radius Depression on Wrist Joint Contact Characteristics, *Journal of Hand Surgery*, **21A** (1996), 554-560.

[7] Hara, T., Horii, E., An, K., Cooney, W.P., Linscheid, R.L. and Chao, E.Y.S.: Force Distribution Across Wrist Joint: Application of Pressure-Sensitive Conductive Rubber, *Journal of Hand Surgery*, **17A** (1992), 339-347.

[8] Kobayashi, M., Berger, R.A., Nagy, L., Linscheid, R.L., Uchiyama, S., Ritt, M. and An, K.: Normal Kinematics of Carpal Bones: A Three Dimensional Analysis of Carpal Bone Motion Relative to the Radius, *Journal of Biomechanics*, **30** (1997), 787-793.

[9] Ruby, L.K., Cooney, W.P., An, K.N., Linscheid, R.L. and Chao, E.Y.: Relative Motion of Selected Carpal Bones: A Kinematic Analysis of the Normal Wrist, *Journal of Hand Surgery*, **13A** (1988), 1-10.

[10] Savelberg, H.H., Otten, J.D., Kooloos, J.G., Huiskes, R. and Kauer, J.M.: Carpal Bone Kinematics and Ligament Lengthening Studied for the Full Range of Joint Movement, *Journal of Biomechanics*, **26** (1993), 1389-1402.

[11] Ishikawa, J., Niebur, G.L., Uchiyama, S., Linscheid, R.L., Minami, A., Kaneda K. and An, K.: Feasibility of Using A Magnetic Tracking Device for Measuring Carpal Kinematics, *Journal of Biomechanics*, **30** (1997), 1183-1186.

[12] Moritomo, H., Viegas, S.F., Elder, K., Nakamura, K., DaSilva, M.F. and Patterson, R.M.: The Scaphotrapezio-Trapezoidal Joint. Part 2: A Kinematic Study, *Journal of Hand Surgery*, **25A** (2000), 911-920.

[13] Patterson, R.M., Nicodemus, C.L., Viegas, S.F., Elder, K.W. and Rosenblatt, J.: High-Speed, Three-Dimensional Kinematic Analysis of the Normal Wrist, *Journal of Hand Surgery*, **23A** (1998), 446-453.

[14] Kaufmann, R.A., Pfaeffle, J., Blankenhorn, B., Stabile, K., Robertson, D. and Goitz, R.: Kinematics of the Midcarpal and Radiocarpal Joints in Radioulnar Deviation: An *In Vitro* Study, *Journal of Hand Surgery*, **30A** (2005), 937-942.

[15] Kaufmann, R.A., Pfaeffle, J., Blankenhorn, B., Stabile, K., Robertson, D. and Goitz, R.: Kinematics of the Midcarpal and Radiocarpal Joint in Flexion and Extension: An *In Vitro* Study, *Journal of Hand Surgery*, **31A** (2006), 1142-1148.

[16] Snel, J.G., Venema, H.W., Moojen, T.M., Ritt, M.J.P.F., Grimbergen, C.A. and den Heeten, G.J.: Quantitative *In Vivo* Analysis of the Kinematics of Carpal Bones From Three-Dimensional CT Images Using A Deformable Surface Model and A Three-Dimensional Matching Technique, *Medical Physics*, **27** (2000), 2037-2047.

[17] Moojen, T.M., Snel, J.G., Ritt, M.J.P.F., Venema, H.W., Kauer, J.M.G. and Bos, K.E.: Scaphoid Kinematics *In Vivo*, *Journal of Hand Surgery*, **27B** (2002), 1003-1010.

[18] Moore, D.C., Crisco, J.J., Trafton, T.G. and Leventhal, E.L.: A Digital Database of Wrist Bone Anatomy and Carpal Kinematics, *Journal of Biomechanics*, **40** (2007), 2537-2542.

[19] Moojen, T.M., Snel, J.G., Ritt, M.J.P.F., Kauer, J.M.G., Venema, H.W., and Bos, K.E.: Three-Dimensional Carpal Kinematics *In Vivo*, *Clinical Biomechanics*, **17** (2002), 506-514.

[20] Genda, E. and Horii, E.: Theoretical stress analysis in wrist joint—neutral position and functional position, *Journal of Hand Surgery*, **25B** (2000), 292–295.

[21] Majima, M., Horii, E., Matsuki, H., Hirata, H. and Genda, E.: Load transmission through the wrist in the extended position, *The American Society for Surgery of the Hand*, **33A** (2008), 182–188.

[22] Gold, G.E., Besier, T.F., Draper, C.E., Asakawa, D.S., Delp, S.L., and Beaupre, G.S.: Weight-Bearing MRI of Patellofemoral Joint Cartilage Contact Area, *Journal of Magnetic Resonance Imaging*, **20** (2004), 526-530.

[23] Bingham, J.T., Papannagari, R., Van de Velde, S.K., Gross, C., Gill, T.J., Felson, D.T., Rubash, H.E., and Li G.: In Vivo Cartilage Contact Deformation in the Healthy Human Tibiofemoral Joint, *Rheumatology*, **47** (2008), 1622-1627.

[24] Li G., Wan L., and Kozanek M.: Determination of Real-Time In-Vivo Cartilage Contact Deformation in the Ankle Joint, *Journal of Biomechanics*, **41** (2008), 128-136.

[25] Pillai, R.R., Thoomukuntla, B., Ateshian, G.A. and Fischer, K.J.: MRI−Based Modeling for Evaluation of *In Vivo* Contact Mechanics in the Human Wrist during Active Light Grasp, *Journal of Biomechanics*, **40** (2007), 2781-2787.

[26] Brechter, J.H. and Powers, C.M.: Patellofemoral Joint Stress During Stair Ascent and Descent in Persons with and without Patellofemoral Pain, *Gait Posture*, **16** (2002), 115-123.

[27] Brechter, J.H., Powers, C.M., Terk, M.R., Ward, S.R. and Lee, T.Q.: Quantification of Patellofemoral Joint Contact Area Using Magnetic Resonance Imaging, *Magnetic Resonance Imaging*, **21** (2003), 955-959.

[28] Besl, P.J. and Mackay, N.: A method for registration of 3-D shapes, *IEEE Transactions on Pattern Analysis and Machine Intelligence*, **14** (1992), 239-256.

[29] Panjabi, M.M., Krag, M.H. and Goel, V.K.: A Technique for Measurement and Description of Three-Dimensional Six Degree-of-Freedom Motion of A Body Joint with An Application to the Human Spine, *Journal of Biomechanics*, **14** (1981), 447-460.

[30] Sasagawa, K., Watanabe, S., Kobayashi, K., Sakamoto, M., Tanabe, Y., Sato, T. and Koga, Y.: Accuracy Examination of Three-Dimensional Bone Surface Model Using MRI and CT, *Journal of Japanese Society for Clinical Biomechanics*, **29** (2008), 397-402 (in Japanese).